ARL-TR-9430 ● APR 2022

DEVCOM ARMY RESEARCH LABORATORY

Tensile Behavior of UHMWPE Solid-State Extrusion (SSE) Film as a Function of Strain Rate

by C Allan Gunnarsson, Stephen L Alexander, and Tusit Weerasooriya

NOTICES

Disclaimers

The research reported in this document was performed in connection with contract/instrument W911QX-16-D-0014 with the DEVCOM Army Research Laboratory.

The findings in this report are not to be construed as an official Department of the Army position unless so designated by other authorized documents. The views and conclusions contained in this document are those of SURVICE Engineering Company and the DEVCOM Army Research Laboratory.

Citation of manufacturer's or trade names does not constitute an official endorsement or approval of the use thereof.

Destroy this report when it is no longer needed. Do not return it to the originator.

ARL-TR-9430 ● APR 2022

Tensile Behavior of UHMWPE Solid-State Extrusion (SSE) Film as a Function of Strain Rate

C Allan Gunnarsson and Tusit Weerasooriya
DEVCOM Army Research Laboratory

Stephen L Alexander
SURVICE Engineering Company

REPORT DOCUMENTATION PAGE		Form Approved OMB No. 0704-0188

1. REPORT DATE *(DD-MM-YYYY)*	2. REPORT TYPE	3. DATES COVERED (From - To)
April 2022	Technical Report	1 October 2019–30 September 2021

4. TITLE AND SUBTITLE	5a. CONTRACT NUMBER
Tensile Behavior of UHMWPE Solid-State Extrusion (SSE) Film as a Function of Strain Rate	5b. GRANT NUMBER
	5c. PROGRAM ELEMENT NUMBER

6. AUTHOR(S)	5d. PROJECT NUMBER
C Allan Gunnarsson, Stephen L Alexander, and Tusit Weerasooriya	5e. TASK NUMBER
	5f. WORK UNIT NUMBER

7. PERFORMING ORGANIZATION NAME(S) AND ADDRESS(ES)	8. PERFORMING ORGANIZATION REPORT NUMBER
DEVCOM Army Research Laboratory ATTN: FCDD-RLW-PB Aberdeen Proving Ground, MD 21005	ARL-TR-9430

9. SPONSORING/MONITORING AGENCY NAME(S) AND ADDRESS(ES)	10. SPONSOR/MONITOR'S ACRONYM(S)
	11. SPONSOR/MONITOR'S REPORT NUMBER(S)

12. DISTRIBUTION/AVAILABILITY STATEMENT

Approved for public release: distribution unlimited.

13. SUPPLEMENTARY NOTES

ORCID IDs: Tusit Weerasooriya, 0000-0003-3299-2166; C Allan Gunnarsson, 0000-0002-8472-5193

14. ABSTRACT

UHMWPE fiber-based protection systems are widely used in blast and impact protection. Ballistic research indicates that UHMWPE film systems may provide equal protection, with greatly reduced cost. To accurately design and model protection systems using UHMWPE film, it is necessary to understand the material properties at the constituent single unidirectional film length scale. Here, experimental techniques have been developed to load UHMWPE at a range of strain rates, including high rate using a tensile Hopkinson bar. Digital image correlation was used to quantify strain in the film. The strain and loading history are used to quantify the rate dependency of the UHMWPE film Young's modulus and strength.

15. SUBJECT TERMS

high-rate loading, digital image correlation, solid-state extrusion, SSE, ultra-high molecular weight polyethylene, UHMWPE, split Hopkinson pressure bar, SHPB, Sciences of Extreme Materials, Terminal Effects

16. SECURITY CLASSIFICATION OF:			17. LIMITATION OF ABSTRACT	18. NUMBER OF PAGES	19a. NAME OF RESPONSIBLE PERSON
a. REPORT	b. ABSTRACT	c. THIS PAGE			C Allan Gunnarsson
Unclassified	Unclassified	Unclassified	UU	32	19b. TELEPHONE NUMBER (Include area code) (410) 306-1964

Contents

List of Figures iv

List of Tables iv

Acknowledgments v

1. Introduction 1

2. Methods 3

2.1 Materials 3

2.2 Quasi-static and Intermediate-Strain Rate Experiments 4

2.3 High-Rate Experiments 5

3. Results 7

3.1 Tensile Young's Modulus 8

3.2 Quasi-static and Intermediate-Strain Rate 9

3.3 High Rate 11

3.4 Strain-Rate Effect on Mechanical Properties 14

4. Discussion and Limitations 15

4.1 Comparison with SSE Film UHMWPE Literature 15

4.1.1 Tensylon at Single UD Ply/Film/Tape Scale 16

4.1.2 Tensylon at Laminate/Plate Scale 17

4.2 High-Rate Experiment Limitations 18

5. Conclusions 18

6. References 19

List of Symbols, Abbreviations, and Acronyms 21

Distribution List 22

List of Figures

Fig. 1 Tensylon film illustrating anisotropic structure along longitudinal direction (roll axis)..... 4

Fig. 2 Loading setup for quasi-static and intermediate-strain rate experiments (scale at right is in inches) 5

Fig. 3 High-strain-rate wrap and clamp film grips and specimen with DIC pattern applied to gage section attached to tensile SHPB..... 7

Fig. 4 (a) Engineering stress vs. DIC strain (Lagrange) and (b) engineering stress and DIC strain (Lagrange) vs. time for high-rate specimen T11 9

Fig. 5 Engineering stress vs. DIC strain (Lagrange) for (a) quasi-static and (b) intermediate-rate specimens..... 10

Fig. 6 DIC strain (Lagrange) profile for quasi-static rate specimen T13 at the image just before failure. The strain profile color map range is 0.00 (purple) – 0.04 (red).. 10

Fig. 7 Loading history (a) and DIC strain (Lagrange) profiles (b) for high-rate specimen T11 during loading at discrete times marked in (a) by blue dots. The color map range is constant for all profiles 0.00 (purple) – 0.10 (red). The incident bar grip is to the left in the (b) images. 11

Fig. 8 Pre-loading (left) and post-failure images (right) for both partially failed specimen T05 (top) and fully failed specimen T07 (bottom) ... 13

Fig. 9 Failure location for six high-rate specimens..... 14

Fig. 10 Tensile behavior for UHMWPE film as a function of strain rate for (a) strength and (b) Young's modulus. The two types of high-rate failure (partial and full) are differentiated by color (a) to show that failure type did not cause noticeable differences in strength. 15

Fig. 11 In-plane Poisson's ratio as a function of strain rate..... 15

List of Tables

Table 1 Summary of material properties averaged for each strain rate 8

Table 2 Tensile Young's modulus and strength of a single UD ply of SSE Tensylon film measured at quasi-static strain rate..... 16

Table 3 The quasi-static tensile Young's modulus and strength of Tensylon, comparing the mesoscale (single UD ply) with the macroscale (laminates)..... 17

Acknowledgments

The authors would like to acknowledge the contributions of the following US Army Combat Capabilities Development Command Army Research Laboratory researchers to this study: Fred Racine and Mike Neblett for fabrication and specimen cutting; and Paul Moy and Daniel O'Brien for technical expertise and consultation.

1. Introduction

Armor systems based on ultra-high molecular weight polyethylene (UHMWPE) fiber composites have been used effectively to provide vehicle protection, as well as dismounted Soldier protection in torso and head protection systems. Recent studies on impact response suggest that UHMWPE films made by solid-state extrusion (SSE) may be an emerging material for use in protection systems. When compared to fiber-based UHMWPE systems, SSE film composites cost less to manufacture and may provide equal or improved protection levels (Singletary and Lauke 2016).

Creation of computational modelling methodology that can predict the ballistic performance of composites based on UHMWPE films requires accurate material properties of the constituent materials. The material properties used must be representative of simulation loading conditions; for SSE UHMWPE films, they also needed to be characterized under tension at high-loading rates, which are representative of loading rates during impact and blast events.

UHMWPE fiber-based protection systems are extensively used throughout the protection community. Common examples include those produced by DSM as the Dyneema HB material series (HB25, HB26, HB80, etc.) and Honeywell (formerly Allied Signal) as the Spectra Shield series. These systems are based on single fibers manufactured through a gel spinning process in which the UHMWPE powder is dissolved in a solvent. The resulting high-strength fiber is combined with a soft matrix material to produce a unidirectional (UD) ply, in which the fibers are aligned in the longitudinal direction. These materials are commercially sold by the roll. The sheet coming off the roll is referred to as the precursor sheet, consisting of two or four UD layers in an alternating 0°/90° configuration. Many studies have been performed to obtain the tensile behavior of UHMWPE single-fiber and fiber-based composites. Sanborn et al. (2015) quantified the loading rate dependence of tensile properties of UHMWPE single fiber (Dyneema SK76) using a direct gripping method. They found that the tensile strength of UHMWPE single fiber was loading rate dependent. Wang et al. (2020) studied the loading rate effect on UHMWPE single yarns, up to a strain rate of 400/s, and found the tensile strength and Young's modulus increased with increasing strain rate from 3.3×10^{-5}/s to 0.33/s but were not dependent on strain rate between 0.33/s and 400/s. Hudspeth et al. (2012) quantified the effect of pre-twist on the tensile strength of UHMWPE single fiber. They found that tensile strength remained unchanged up to a shear strain of 14%, and decreased linearly with increased shear strain, for quasi-static (0.01/s) and high (600/s) tensile strain rates. Russell et al. (2013) quantified the tensile response of

UHMWPE single fiber, and fiber-based yarns and laminates over a range of strain rates of up to 10^3/s.

However, UHMWPE fiber systems are costly due to the use and reclamation of solvent during the manufacturing process (Weedon 2001). UHMWPE films (also referred to as tapes) are less expensive to manufacture when compared with fiber-based systems because they allow for elimination of the solvent from the manufacturing process (van der Werff and Heisserer 2016). Instead of dissolution in a solvent, the UHMWPE powder is dry extruded, and then drawn into a high-strength film, in the SSE process (Jordan et al. 2002). Not using solvent can provide substantial cost savings. As an example, Reddy et al. (2020) produced panels with different ratios of SSE-film-based precursors and fiber-based precursors. At equal areal density, the panel they produced from 100% fiber-based material was 70% more costly to manufacture than the panel produced from 100% film-based material.

Although less expensive, the relative ballistic performance of UHMWPE film-based armor compared to fiber-based armor is not well understood at this time. The few comparative studies in literature indicate that the film-based material decreases V50 (Frietas et al. 2014) and energy absorbed during impact (Reddy et al. 2020), which corresponds to poorer performance. However, film-based armor was consistently found to have lower backface deformation (BFD) than fiber-based armor in both previously referenced studies as well as in a recent study by Cline and Love (2020). Lower values of BFD are desirable to decrease the risk of behind armor blunt trauma.

Therefore, additional studies on the mechanical response of these advanced materials are required to take advantage of both cost savings and any potential ballistic improvements. The mechanical properties of films consolidated via hot compaction have been characterized for strength, stiffness, and hardness (Hine et al. 2001, Orench et al. 2006, Hine et al. 2011). Others have investigated the mechanical properties of laminates made by consolidating SSE films in a [0/90] layup configuration. O'Masta et al. (2016) compared laminate panels produced from fiber-based sheets and film-based material and found that the film-based plies had lower tensile strength.

Understanding the mechanical behavior at the mesolength scale of the single film/ply at relevant high-strain rate impact events will allow for incorporation of material properties into computational models that are constructed around the single-film component. Such mesoscale computational frameworks can assist with understanding the ballistic performance by elucidating the underlying deformation and failure mechanisms, as demonstrated for the case of fiber-based composites by

Liu et al. (2019). While there is an appreciable body of work on fiber-based UHMWPE material, there is much less literature on the mechanical characterization of UHMWPE SSE films at the mesoscale of the single ply. Alil et al. (2017) and Hine et al. (2001) quantified the tensile properties for single UD SSE films as part of larger experimental studies. The authors are aware of only one study that exists in literature to study the effect of strain rate on the single UD film. Zhou et al. (2021) studied the tensile properties of Dyneema UHMWPE SSE film as a function of strain rate using a pressurized ring specimen to generate circumferential tension. They reported strain rate dependency for both stiffness and strength, with both increasing as strain rate increased.

In this study, the tensile behavior of DuPont's Tensylon UHMWPE SSE UD film was studied as a function of loading rate. Novel direct grips were developed to assist in loading the film at high-strain rate using a tensile Hopkinson bar, while using capstan grips for textiles to load the film at quasi-static and intermediate-strain rates. High-speed imaging was used to observe the speckled film during high-rate loading. Digital image correlation (DIC) was used to obtain specimen surface strain, including at high-strain rate. This measured direct strain was used with loading history to obtain the material Young's modulus and strength, as a function of strain rate. The results of this study will allow for accurate constitutive models that incorporate strain rate sensitivity to be used in computational simulations of threat–target interactions based on this material. Here, the experimental techniques and results are discussed.

2. Methods

2.1 Materials

The UHMWPE SSE UD film used in this study was trade named Tensylon, which is manufactured by DuPont. This film is used in production of their Tensylon HBSD 30A product with two UD layers (0/90).

The SSE process causes a preferential alignment along the roll axis; this structure can be observed visually in Fig. 1. The UD film is highly anisotropic, with almost zero transverse strength; the film can be split along the roll direction easily by hand. The UD film roll was approximately 60 μm thick, and 228.6 mm wide. From this roll, individual tensile specimens were cut using a Gerber table cutter. Here, specimen length indicates the longitudinal length of the specimen along the roll axis (Fig. 1, x-axis), while specimen width refers to the transverse dimension (Fig. 1, y-axis).

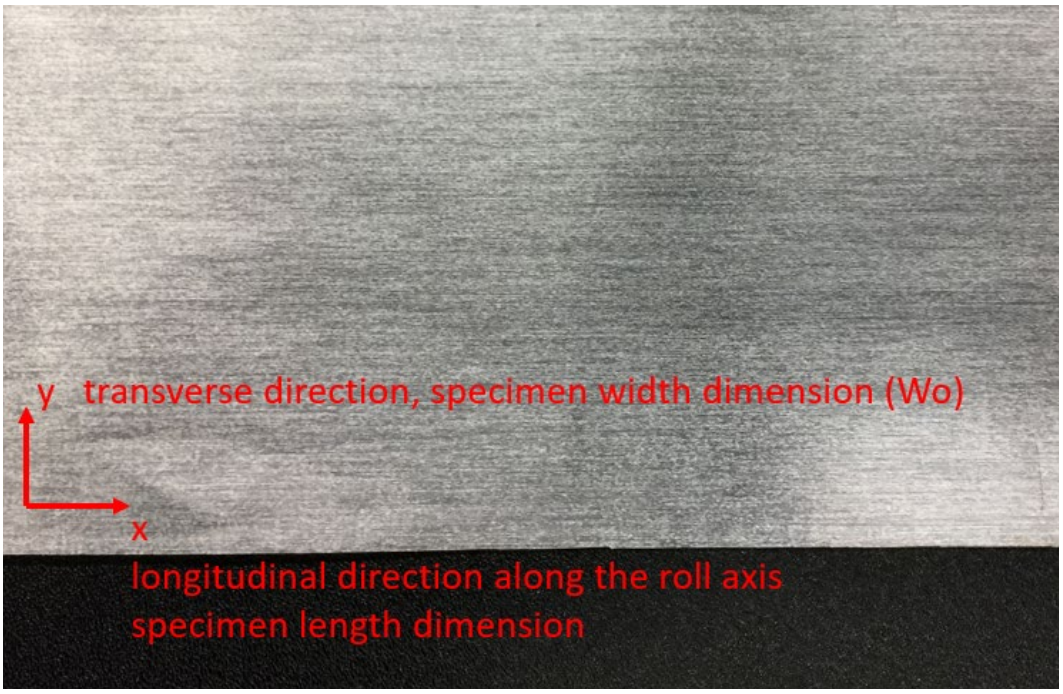

Fig. 1 Tensylon film illustrating anisotropic structure along longitudinal direction (roll axis)

2.2 Quasi-static and Intermediate-Strain Rate Experiments

For the quasi-static and intermediate-strain rate experiments, a servo–hydraulic Instron test frame was used with capstan grips for textiles to load the specimens. The specimens were cut to 1.83 m (72.0 inch) long and 25.4 mm (1.0 inch) wide. The specimens were wrapped around the capstan grips with four loops on the moving grip and three loops on the stationary grip. This loading setup resulted in a specimen gage length of approximately 5 inches not in contact with the grip. During loading, the specimen did deform slightly in the grip. Due to this slip that occurred, specimen strain was obtained using DIC. An average strain using the Lagrange strain tensor was extracted over the entire specimen gage length. The experimental setup for the quasi-static and intermediate-strain rate experiments is shown in Fig. 2, with specimen, DIC speckle, and grips. For these experiments, the specimens were first coated with white paint and black speckles added. At both quasi-static and intermediate-strain rates, a framing camera captured the specimen during loading. For the quasi-static rate experiments, a FLIR 12.3-megapixel camera at 2 fps was used, and at intermediate rate, a Photron SA-5 1.0-megapixel camera at 500 fps was used.

For quasi-static strain rate, the target strain rate was 0.001/s. However, due to the slip that occurred, several different crosshead velocities were used to obtain the target strain rate, from 0.15 to 1.5 mm/s. For the intermediate-strain rate, a range of crosshead velocities from 320 to 480 mm/s were used, corresponding to strain rates of 0.375 to 0.5/s.

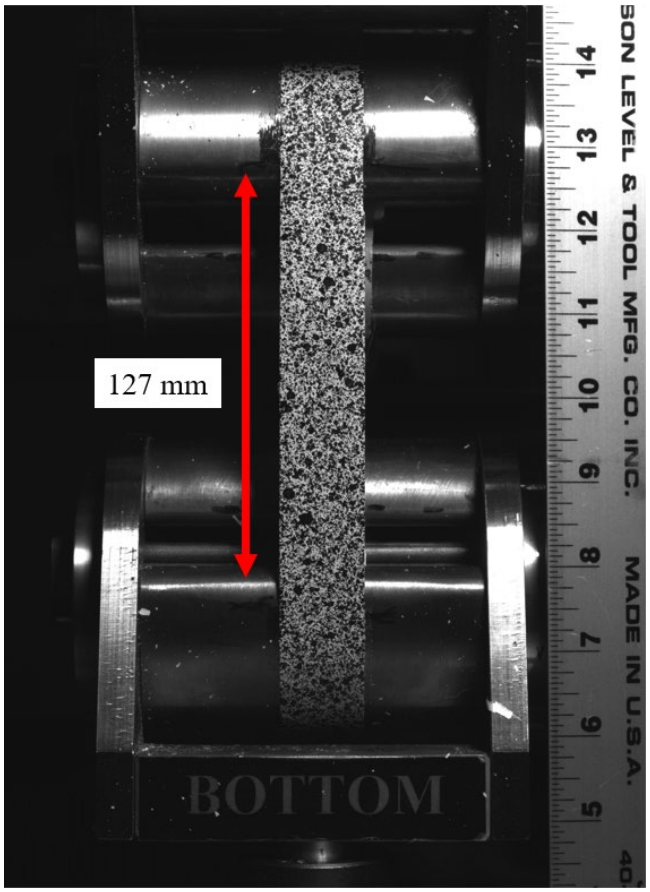

Fig. 2 Loading setup for quasi-static and intermediate-strain rate experiments (scale at right is in inches)

2.3 High-Rate Experiments

High-strain-rate tensile experiments were performed on the UHMWPE film using a tensile split Hopkinson pressure bar (SHPB) setup. Details of the setup follow. The operation and theory of the tensile SHPB are omitted for brevity; however, extensive literature covering this topic does exist (Chen and Song 2010). The SHPB setup consisted of a 457 mm long tubular striker impacting a flanged 2.75 m Maraging 300 steel incident bar and a 1.83 m transmission bar of the same material. The incident and transmission bar have threaded ends at the specimen interface and film grips were threaded into the bar ends. Both bars used strain gages to measure the stress waves in the bars during loading. The transmission bar used both resistive

and semiconductor strain gages to measure the transmitted stress signal. With the low force required for specimen failure, only the semiconductor strain gages provided a measure of the transmitted bar stress pulse. Semiconductor gages are known to be highly sensitive to environmental conditions; here, they were calibrated with the stable resistive gages using a threaded Maraging 300 steel adapter that connected the two bars together to form a single bar.

To grip the film specimens properly at high rate, several iterations of grip design were investigated. Discarded designs included grips using either sharp teeth or blunt rounded teeth, and direct friction clamping without any teeth. With these designs, specimens either slipped prior to failure, or failed prematurely at the grip interface (sharp teeth). The final film grip design used a wrap and clamp design. The grips consisted of two pieces: the main grip and the grip clamp. The film specimen was wrapped around the grip clamp for three loops and the grip clamp was fastened to the main grip using eight bolts (Fig. 3). Procedures were established and followed to ensure that the specimen was tightly wrapped around the grip clamp and aligned parallel to the bar axis. Film specimens of total length 650 mm and width 3.175 mm were used, with a resulting approximate nominal gage length of 10–20 mm. This gage length was varied across several experiments to investigate gage length dependence on the failure behavior (discussed later). A Shimadzu HPV-2 ultra-high-speed camera was used at either 250K or 500K fps to image the specimen during loading, allowing for postprocessing of these images to obtain specimen strain using DIC software (Correlated Solutions VIC-2D). The specimens were speckled with only black paint, using the natural background film surface color for high contrast. High-intensity LED lights were used to illuminate the specimen during loading; to avoid any heating of the specimen, these lights were turned on just prior to loading. An average axial strain using the DIC software Lagrange strain tensor was extracted from the entire specimen gage length.

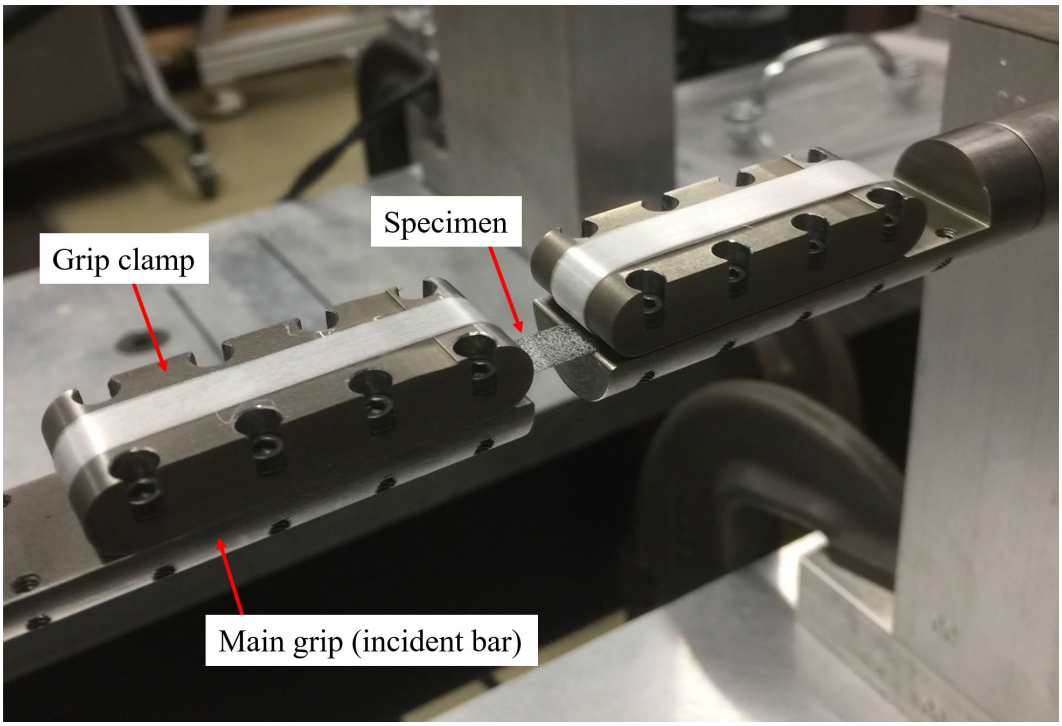

Fig. 3 High-strain-rate wrap and clamp film grips and specimen with DIC pattern applied to gage section attached to tensile SHPB

3. Results

Section 3.1 describes how the tensile Young's modulus was obtained for each experiment. The mechanical response and specimen behavior for the intermediate- and quasi-static strain rate experiments are presented in Section 3.2. Section 3.3 describes the mechanical response and failure behavior for the high-strain-rate experiments. The average results for each strain rate are summarized in Table 1 and are also presented in Section 3.4. Seven specimens were used for both quasi-static and intermediate-strain rate. For high-strain rate, 22 specimens were tested; of these, 4 experienced full failure and 18 experienced partial failure. These two failure types are defined and discussed in Section 3.3. Full failure refers to when failure occurred across the entire specimen width; partial failure refers to when 60%~80% of the specimen width failed. For the tensile experiments, there are two specimen numbering sets: the high-rate experiments number from T01 to T26, while the quasi-static and intermediate-rate experiments number from T01 to T22. When referred to here by specimen number, the specimen strain rate is also specified for clarity.

Table 1 Summary of material properties averaged for each strain rate

Strain rate		No. Specs. (n)	Strength (GPa)		Young's modulus (GPa)		Strain rate (/s)		Poisson's ratio	
			Average	Standard deviation	Average	Standard deviation	Average	Standard deviation	Average	Standard deviation
Quasi-static		7	1.24	0.14	102.1	14.8	0.00076	0.000522	0.319	0.0221
Intermediate		7	1.47	0.13	114.9	12.3	0.44229	0.044	0.191	0.0513
High	Full failure[a]	4	1.83	0.15	133.7	33.9	339.8	70.5	0.401	0.1809
	All failure	22	1.89	0.20	140.6	32.4	252.6	71.6	0.349	0.1704

[a] The high-rate experiments exhibited two types of failure: full failure and partial failure, as defined in Section 3.3. Full failure refers to when failure occurred across the entire specimen width. Partial failure refers to when 60%~80% of the specimen width failed.

3.1 Tensile Young's Modulus

The tensile Young's modulus was obtained for each specimen. For the quasi-static and intermediate-rate experiments, a linear fit was obtained for the stress–strain response of each specimen over the strain range 0.000–0.005 (0%–0.5%).

For the high-rate experiments, the strain history data was noisy, leading to difficulty in constructing stress–strain relationships. When it was possible to extract a Young's modulus, this modulus was very sensitive to selection of data points, as each experiment consisted of a small number of images (~20 for 250K fps, ~40 for 500K fps) during loading. The stress–strain response for one high-rate specimen (T11) is shown in Fig. 4a using strain data obtained with DIC and is typical for the high-rate specimens. Therefore, the Young's modulus was estimated using the loading (stress) rate and strain rate for all of the high-rate specimens. The loading rate was obtained by taking a linear fit of the stress history after any initial tightening of the specimen and before any softening prior to failure. The strain rate was obtained by using a linear fit of the strain history during loading. The Young's modulus was calculated as loading rate divided by the strain rate. Figure 4b shows the loading and strain history for high-rate specimen T11. In the figure, the linear portion of the loading history and the strain history used to calculate loading and strain rate are shown by the dashed linear fit lines.

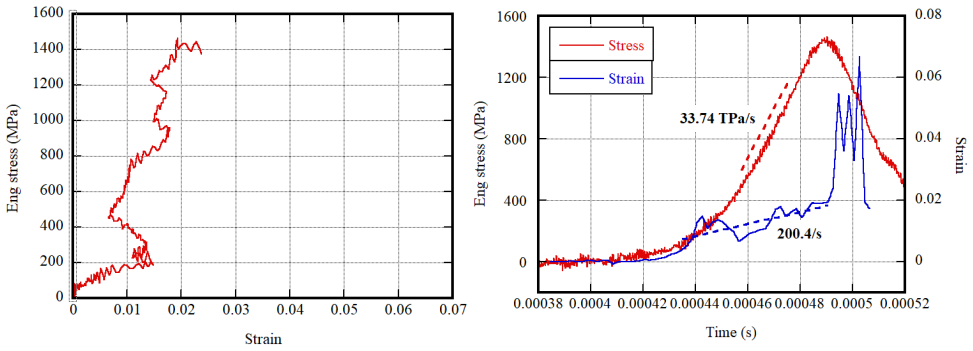

Fig. 4 (a) Engineering stress vs. DIC strain (Lagrange) and (b) engineering stress and DIC strain (Lagrange) vs. time for high-rate specimen T11

3.2 Quasi-static and Intermediate-Strain Rate

The engineering stress versus DIC strain (Lagrange) response for all specimens is shown for quasi-static (Fig. 5a) and intermediate- (Fig. 5b) strain rates. A typical DIC strain distribution for the image just prior to failure for quasi-static experiment T13 is shown in Fig. 6. For both rates, the modulus decreased with the loading.

For some of the quasi-static specimens (T07, T10, T12), small local partial failures occurred as small filament groups failed. These partial failures caused slight load drops but were followed by continued load increase until complete failure of each specimen as shown in Fig. 5a (red, blue, black).

At quasi-static strain rate, there was a minimal initial slip as the film specimens tightened against the grips and then began linear loading. In addition to this initial slip, four quasi-static specimens (T10, T11, T12, T13) also slipped in the grips once a certain load level was achieved, although stress continued to increase until failure. This no-slip followed by slip caused the specimens to experience two strain rates: one during the no-slip region followed by a lower strain rate during the slip region. The machine displacement rate remained constant during the experiment. For the four specimens that experienced this slip, the initial strain rate during the no-slip region is reported in Table 1. Generally, slippage between the specimen and the grip is not expected to affect, or be seen in, the stress–strain response (Fig. 5a) because it would affect both the stress and strain response simultaneously and because strain was measured by DIC. Therefore, the decrease in modulus observed in Fig. 5a is considered a true material response, unconnected with the experimental conditions.

For the intermediate-strain rate, no slip was observed other than initial tightening of the specimen against the grips. The strain rate remained constant over the loading history.

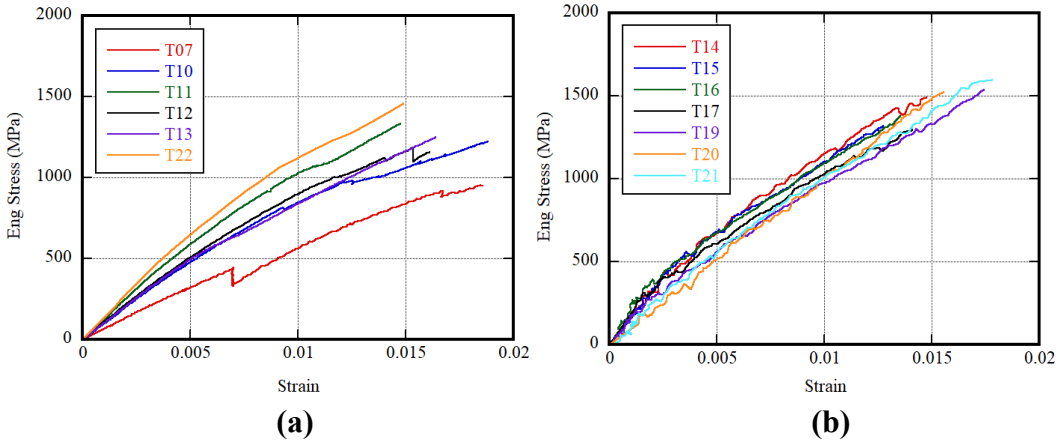

Fig. 5 Engineering stress vs. DIC strain (Lagrange) for (a) quasi-static and (b) intermediate-rate specimens

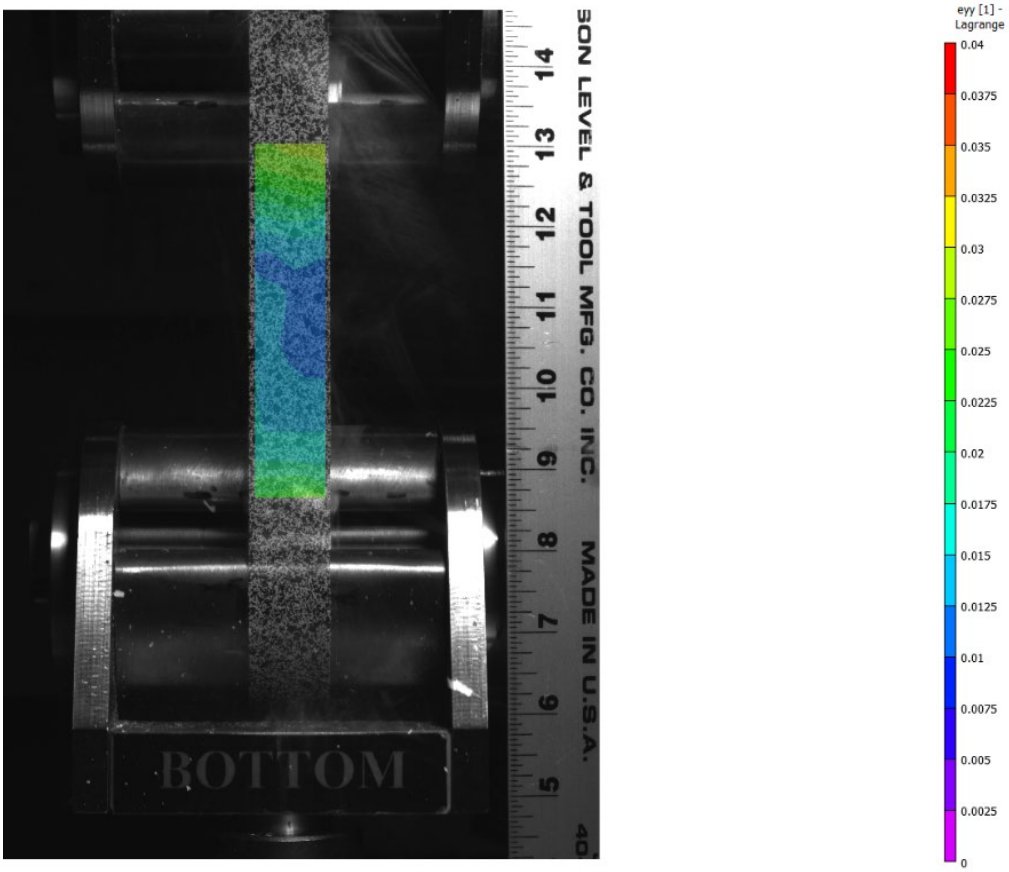

Fig. 6 DIC strain (Lagrange) profile for quasi-static rate specimen T13 at the image just before failure. The strain profile color map range is 0.00 (purple) – 0.04 (red).

3.3 High Rate

The film specimens were loaded at high rate using a wrap and clamp grip design. This minimized any specimen slip during loading and caused specimen failure during the initial loading pulse. The loading history for high-rate specimen T11 is shown in Fig 7, along with a series of DIC strain profiles at discreet time points during loading and after failure. The blue dots represent the timing of the accompanying strain profile. In the images, the incident bar grip is at the left and the transmission bar grip is at the right. As seen from the images, the strain field is reasonably distributed and not concentrated at any single location. In addition, the full width of the specimen is deformed even though the bottom section of the specimen is where partial failure occurred. For these experiments, about 50–60 images were acquired between load onset and max load; only a small selection are shown in Figs. 7a and 7b.

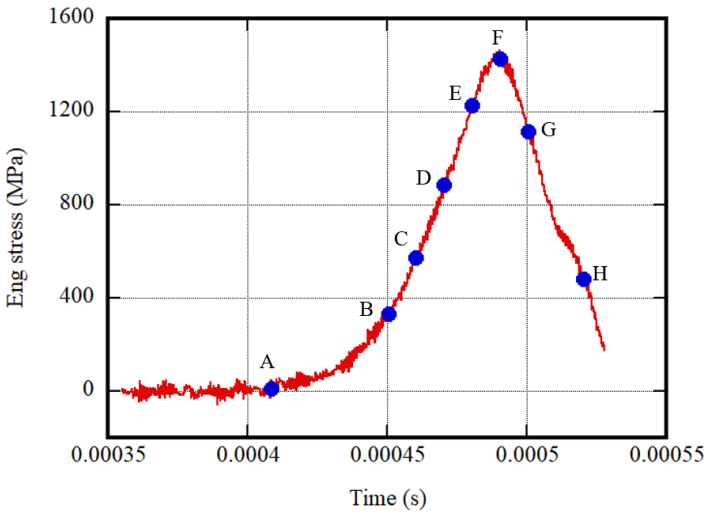

(a)

Fig. 7a Loading history (a) and DIC strain (Lagrange) profiles (b) for high-rate specimen T11 during loading at discrete times marked in (a) by blue dots. The color map range is constant for all profiles 0.00 (purple) – 0.10 (red). The incident bar grip is to the left in the (b) images.

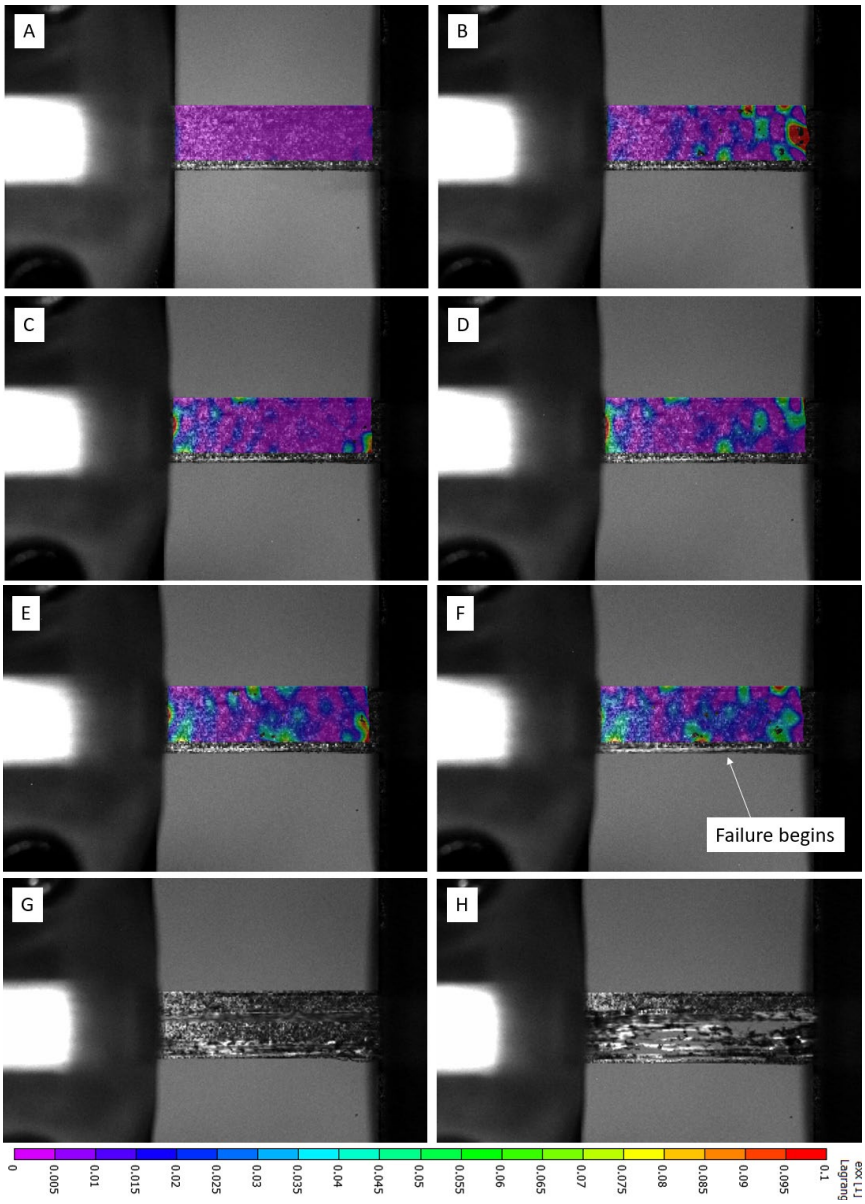

(b)

Fig. 7b Loading history (a) and DIC strain (Lagrange) profiles (b) for high-rate specimen T11 during loading at discrete times marked in (a) by blue dots. The color map range is constant for all profiles 0.00 (purple) – 0.10 (red). The incident bar grip is to the left in the (b) images.

Failure Behavior

The film specimens exhibited two failure behavior types at high rate. These two different types are referred to as either full or partial failure, with examples shown in Fig. 8. For most of the specimens (n = 18), load increased to a maximum at which point failure occurred across a large but incomplete percentage of the specimen width, within 60%–80% of the original preloaded width (W_o). This failure type is referred to as partial failure; for this failure, the failed width (W_f) is used to calculate

tensile strength. For 20% of the specimens (n = 4), failure occurred across the entire specimen width. This failure type is referred to as full failure; for these experiments, the full specimen width (W_o) prior to loading is used for calculation of strength. The specimen gage length was varied slightly between 10 and 20 mm to determine if there was an effect of gage length on failure types. However, failure type did not appear to be affected by gage length. Specimen failure type appeared to be random, which was most likely based on slight differences in specimen alignment during loading into the grip and clamping.

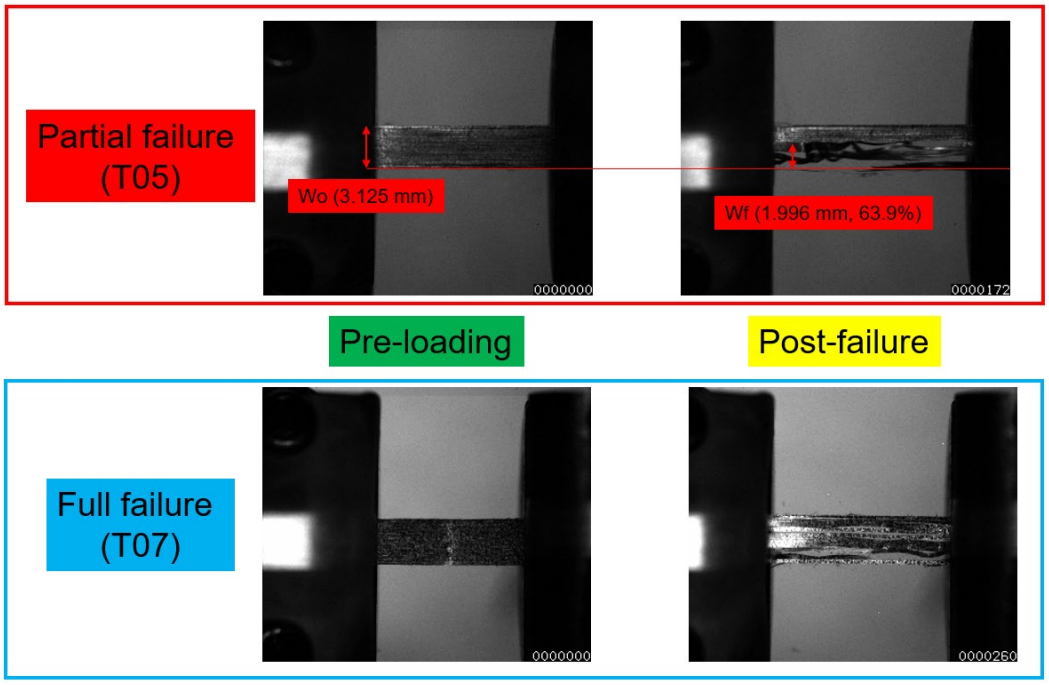

Fig. 8 Pre-loading (left) and post-failure images (right) for both partially failed specimen T05 (top) and fully failed specimen T07 (bottom)

Failure location in the high-rate specimens was observed using high-speed imaging for most specimens. Some specimens clearly failed within the gage length, while others failed at the grip–specimen interface. Figure 9 shows a sample of failure locations for several different specimens. In all images, the incident bar grip is at the left of the image and the transmission bar grip is at the right. During loading, filament groups aligned along the roll direction would split apart. In Figs. 8 and 9, this splitting is seen as horizontally aligned failure—in contrast to tensile failure occurring in the vertical direction.

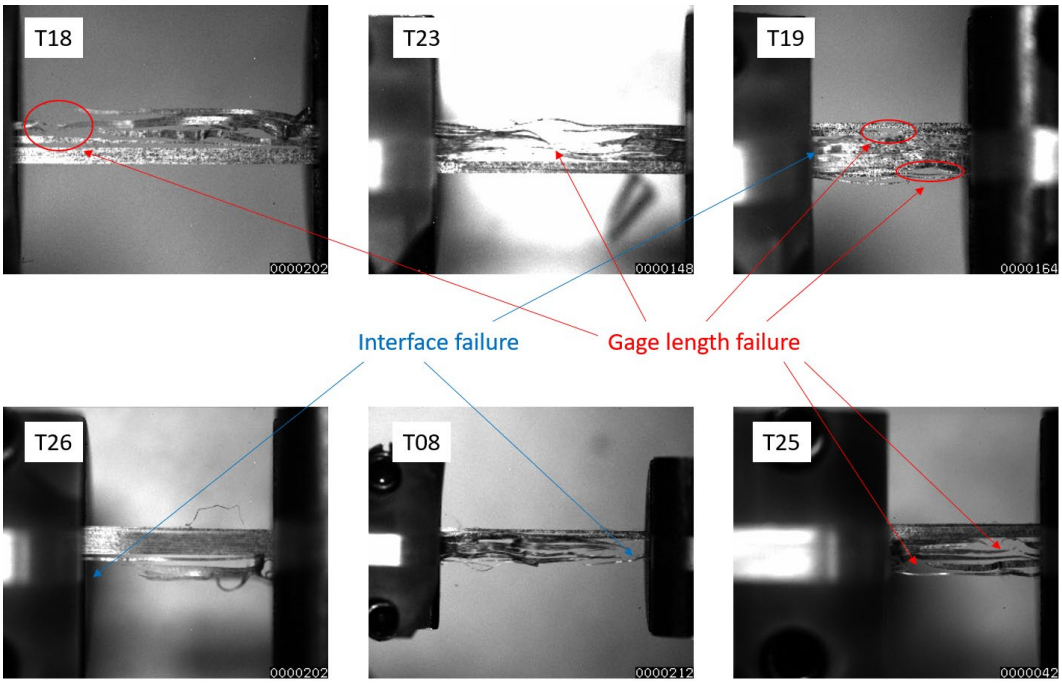

Fig. 9 Failure location for six high-rate specimens

3.4 Strain-Rate Effect on Mechanical Properties

The experimental results documented here indicate that tensile strength and stiffness of UHMWPE film demonstrates strain-rate sensitivity; increasing strain rate corresponds to increased strength and Young's modulus. The individual specimen and rate-averaged strength results from the tensile experiments for each of the three strain rates are shown in Fig. 10a, while the individual specimen and rate-averaged Young's modulus results for each of the three strain rates are shown in Fig. 10b.

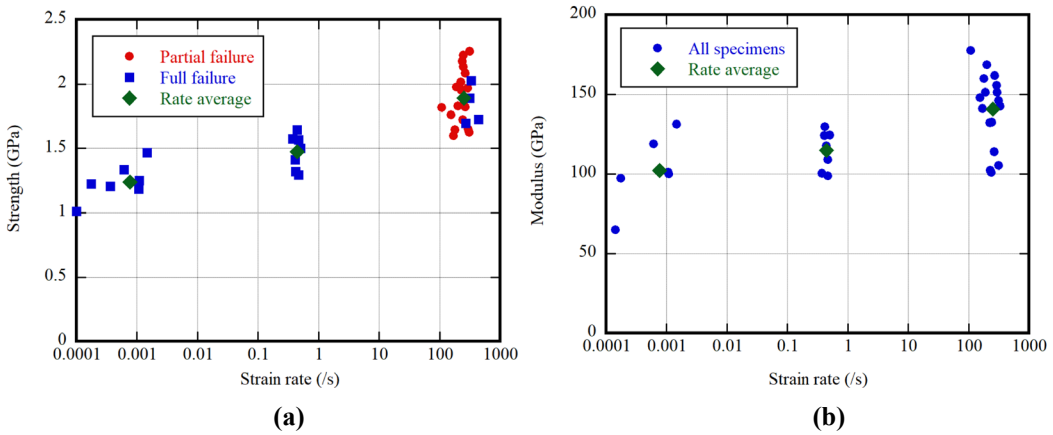

Fig. 10 Tensile behavior for UHMWPE film as a function of strain rate for (a) strength and (b) Young's modulus. The two types of high-rate failure (partial and full) are differentiated by color (a) to show that failure type did not cause noticeable differences in strength.

The in-plane Poisson's ratio was also calculated for most of the experiments by analysis of the DIC-calculated strain profiles for both axial and transverse strain. However, for several specimens, the transverse strain was very noisy; those specimens were omitted from the data set. Figure 11 shows the individual and rate-averaged Poisson's ratio as a function of strain rate. In contrast to the Young's modulus and strength, the Poisson's ratio did not show clear trends with strain rate.

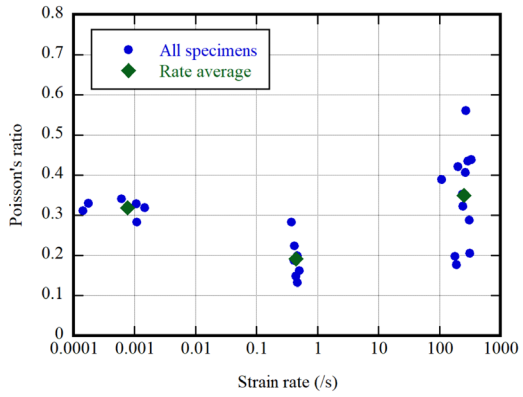

Fig. 11 In-plane Poisson's ratio as a function of strain rate

4. Discussion and Limitations

4.1 Comparison with SSE Film UHMWPE Literature

In this section, the mechanical properties obtained in the current study are compared with previous literature that also characterized SSE UHMWPE films. While there have been numerous studies on gel-spun, fiber-based UHMWPE materials, only a few studies have characterized the newer SSE UHMWPE films such as Tensylon.

This section is divided into two parts based on length scale of the characterized material published in other studies. First, Section 4.1.1 focuses on studies that included data at the length scale of the single UD film ply or tape—as in the present study. Next, the effect of moving up in length scale from the single UD ply to the composite scale is examined in Section 4.1.2, which compares the Tensylon UD film of the current study with previous studies that characterized Tensylon at the macroscale of laminates.

4.1.1 Tensylon at Single UD Ply/Film/Tape Scale

For the quasi-static strain rate, the experimental properties obtained here agree well with other studies that also reported tensile properties for single UD plies of Tensylon, as shown in Table 2. The Young's modulus reported here may be slightly higher due to the use of a smaller strain range to obtain Young's modulus. Other studies investigating the strain-rate effect on UHMWPE single fiber, filaments, and laminates also show rate effects on tensile strength (Hudspeth et al. 2012, Russel et al. 2013, Sanborn et al. 2015, Wang et al. 2020).

Table 2 Tensile Young's modulus and strength of a single UD ply of SSE Tensylon film measured at quasi-static strain rate

Study	SSE Film Material	Strain Rate (/s)	Ply Tensile Young's Modulus (GPa)	Ply Tensile Strength (GPa)
Current	UD Tensylon plies supplied by DuPont	7.6×10^{-4}	102	1.2
Alil et al. 2017	UD Tensylon plies derived[a] from Tensylon HSBD 30A	8.3×10^{-4}	60~90[b]	1.0~1.2[b]
Cain et al. 2021	Tensylon HSBD 30A laminates[c]	2.6×10^{-3}	83	(not included)
O'Masta et al. 2016	Tensylon HSBD 30A laminates[d]	10^{-3}	(not included)	1.2
Hine et al. 2001	UD Tensylon plies supplied by Synthetic Industries, USA	10^{-3}	88	(not included)

[a] Tensylon HSBD 30A is the commercial version of Tensylon sold by DuPont. It consists of two plies of UD Tensylon in a 0°/90° configuration, joined with an adhesive layer. Alil et al. (2017) detached one ply from the other to characterize single UD plies.
[b] Approximated from the linear portion of the stress–strain responses.
[c] Cain et al. (2021) characterized the tensile response of different laminate configurations of Tensylon HSBD 30A and used an inverse optimization procedure to analytically derive ply-level parameters.
[d] O'Masta et al. (2016) characterized the tensile response of $[0/90]_n$ laminates of Tensylon HSBD 30A and multiplied the tensile strength of the $[0/90]_n$ laminate by 2 to calculate the tensile strength of the single UD ply.

4.1.2 Tensylon at Laminate/Plate Scale

Table 3 compares the Tensylon UD plies from the current study with previous studies that characterized laminates (plates) fabricated from Tensylon. The comparison shows that the tensile properties of the single UD ply measured in the current study are approximately twice the corresponding properties of laminates. This could be expected for $[0/90]_n$ laminates where only half of the plies have their preferential direction aligned with the applied tensile strain. However, the reduction in properties is also seen in UD laminates formed with all plies in the same direction. Therefore, the reduction in mechanical properties may be related to a more fundamental change in the structure or performance of the SSE UHMWPE film due to the processing (temperature, pressure, time) involved in forming the laminates.

Table 3 The quasi-static tensile Young's modulus and strength of Tensylon, comparing the mesoscale (single UD ply) with the macroscale (laminates)

Study	SSE Film Material	Strain Rate (/s)	Tensile Young's Modulus (GPa)	Tensile Strength (GPa)
Current	UD Tensylon **plies** supplied by DuPont	7.6×10^{-4}	102	1.2
Alexander and Weerasooriya 2021	$[0/90]_n$ **laminate** made from Tensylon HSBD 30A[a]	(ultrasonic measurement)	60	(not measured)
Alil et al. 2017	$[0/90]_n$ **laminates** made from Tensylon HSBD 30A[a]	Quasi-static (not specified)	30~40[b]	0.4~0.5[b]
O'Masta et al. 2016	$[0/90]_n$ **laminate** made from Tensylon HSBD 30A[a]	10^{-3}	50[a]	0.6[a]
Hine et al. 2001	UD **laminates** made by consolidating UD Tensylon plies supplied by Synthetic Industries, USA[c]	10^{-3}	45-69[d]	(not included)

[a] Three of the previous studies (O'Masta et al. 2016, Alil et al. 2017, Alexander and Weerasooriya 2021) documented in Table 3 fabricated the laminates from the form of Tensylon that is commercially available from the current manufacturer, DuPont. This product, marketed as Tensylon HSBD 30A, is shipped by the roll. The sheet coming off the roll consists of two plies oriented in the 0°/90° direction and joined by an adhesive layer. Several of these sheets were then consolidated to produce $[0/90]_n$ laminates.

[b] Approximated from the initial portion of the stress–strain responses.

[c] Hine et al. (2001) produced UD laminates by consolidating UD plies of Tensylon, which they obtained directly from a previous Tensylon manufacturer.

[d] Range was due to different processing temperatures.

4.2 High-Rate Experiment Limitations

Traditional valid Hopkinson bar high-rate experiments require a state of specimen equilibrium during loading. Here, that condition was not able to be verified for these experiments. The large mass of the grip system contributed a large inertial loading at the incident bar–specimen interface. Additionally, the large impedance mismatch between specimen and grip meant that the incident and reflected pulses were almost identical, causing the specimen–incident bar grip data to be very noisy. However, the measurement of strain on the specimen surface indicated that deformation was distributed across the gage length, suggesting that the stress state was approximately constant across the specimen.

The strain rates obtained here are lower than normally reported for high rate. This is due to the long gage lengths caused by the high-rate grip geometry, as well as possible tightening of the specimen in the grip during loading.

5. Conclusions

UD Tensylon UHMWPE SSE film was successfully loaded in tension to failure at quasi-static, intermediate-, and high-strain rates, using a novel gripping system that prevented slip and promoted specimen failure in the gage length. The film tensile strength exhibited a strain-rate effect, with increasing strain rate corresponding to increasing strength. The strength increased from 1.24 GPa to 1.89 GPa as strain rate increased from 10^{-3}/s to 250/s. A similar effect was observed for the film Young's modulus, which increased from 100 GPa to 140 GPa as strain rate increased from 10^{-3}/s to 250/s. The results of this study will allow for more accurate constitutive and failure models that incorporate strain-rate sensitivity to be used in computational simulations of threat–target interactions based on this material.

6. References

Alexander SL, Weerasooriya T. Mechanical characterization of Advanced Ultra-High Molecular Weight Polyethylene (UHMWPE) composites by ultrasonic method. DEVCOM Army Research Laboratory (US); 2021 Aug. Report No.: ARL-TR-9254.

Alil LC, Arrigoni M, Badea SM, Barbu C, Istrate M, Mostovykh PS. On the constitutive law for the mechanical quasi-static response of criss-cross composites (on the example of UHMWPE). Hum Factors Mech Eng Defense Safety. 2017;1(1):1–12.

Cain JJ, Staniszewski JM, Bogetti TA. Modeling the nonlinear behavior of UHMWPE laminates using optimized ply-level properties with stepwise fiber-angle rotations. DEVCOM Army Research Laboratory (US); 2021 Aug. Report No.: ARL-TR-9264.

Chen WW, Song B. Split Hopkinson (Kolsky) bar: design, testing and applications. Springer Science & Business Media; 2010 Nov 11.

Cline J, Love B. The effect of in-plane shear properties on the ballistic performance of polyethylene composites. Int J Impact Eng. 2020;143:103592.

Hine PJ, Ward IM, Jordan ND, Olley RH, Bassett DC. A comparison of the hot-compaction behavior of oriented, high-modulus, polyethylene fibers and tapes. J Macromol Sci B. 2001;40(5):959–89.

Hine PJ, Unwin AP, Ward IM. The use of an interleaved film for optimising the properties of hot compacted polyethylene single polymer composites. Polymer. 2011;52(13):2891–8.

Hudspeth M, Nie X, Chen W. Dynamic failure of Dyneema SK76 single fibers under biaxial shear/tension. Polymer. 2012;53(24):5568–74.

Jordan ND, Olley RH, Bassett DC, Hine PJ, Ward IM. The development of morphology during hot compaction of Tensylon high-modulus polyethylene tapes and woven cloths. Polymer. 2002;43(12):3397–404.

Liu BG, Wadley HN, Deshpande VS. Failure mechanism maps for ultra-high molecular weight polyethylene fibre composite beams impacted by blunt projectiles. Int J Solids Struct. 2019;178:180–198.

O'Masta MR, Crayton DH, Deshpande VS, Wadley HN. Indentation of polyethylene laminates by a flat-bottomed cylindrical punch. Compos Part A Appl Sci Manuf. 2016;80:138–147.

Orench IP, Calleja FB, Hine PJ, Ward IM. A microindentation study of polyethylene composites produced by hot compaction. J Applied Polym Sci. 2006;100(2):1659–63.

Reddy PR, Reddy TS, Srikanth I, Kushwaha J, Madhu V. Development of cost effective personnel armour through structural hybridization. Defence Tech. 2020;16(6):1089–97.

Russell BP, Karthikeyan K, Deshpande VS, Fleck NA. The high strain rate response of ultra high molecular-weight polyethylene: from fibre to laminate. Int J Impact Eng. 2013;60:1–9.

Sanborn B, DiLeonardi AM, Weerasooriya T. Tensile properties of Dyneema SK76 single fibers at multiple loading rates using a direct gripping method. J Dynam Behav Mater. 2015;1(1):4–14.

Singletary J, Lauke B. Polyolefin film–reinforced composites for personal protection. Advanced Fibrous Composite Materials for Ballistic Protection. Woodhead Publishing; 2016 Jan 1. p. 389–408.

van der Werff H, Heisserer U. High-performance ballistic fibers: ultra-high molecular weight polyethylene (UHMWPE). Advanced fibrous composite materials for ballistic protection Woodhead Publishing; 2016 Jan 1. p. 71–107.

Wang H, Hazell PJ, Shankar K, Morozov EV, Jovanoski Z, Brown AD, Li Z, Escobedo-Diaz JP. Tensile properties of ultra-high-molecular-weight polyethylene single yarns at different strain rates. J Compos Mater. 2020;54(11):1453–66.

Weedon G. High-performance fibres. In: Hearle JW, editor. Elsevier; 2001 Oct 26. p. 132–155).

Zhou J, Heisserer U, Duke PW, Curtis PT, Morton J, Tagarielli VL. The sensitivity of the tensile properties of PMMA, Kevlar and Dyneema to temperature and strain rate. Polymer. 2021;225:123781.

List of Symbols, Abbreviations, and Acronyms

ARL	Army Research Laboratory
BFD	backface deformation
DEVCOM	US Army Combat Capabilities Development Command
DIC	digital image correlation
fps	frames per second
LED	light-emitting diode
SHPB	split Hopkinson pressure bar
SSE	solid-state extrusion
UD	unidirectional
UHMWPE	ultra-high molecular weight polyethylene

1 (PDF) DEFENSE TECHNICAL INFORMATION CTR
DTIC OCA

1 (PDF) DEVCOM ARL
FCDD RLD DCI
TECH LIB

12 (PDF) DEVCOM SC
MG CARBONI
D COLANTO
R DILLALLA
B FASEL
J FONTECCHIO
B KIMBALL
J KIREJCZYK
J PARKER
M MAFEO
M MARKEY
D OTTERSON
D PHELPS

2 (PDF) PEO SOLDIER
J HOPPING
J MULLENIX

1 (PDF) PEO IEWS
A FOURNIER

1 (PDF) MTRL SCIENCES DIV
LAWRENCE BERKELY NATL LAB
R RITCHIE

5 (PDF) SOUTHWEST RSRCH INST
C ANDERSON JR
S CHOCRON
D NICOLELLA
T HOLMQUIST
G JOHNSON

2 (PDF) NIST
A FORSTER
M VANLANDINGHAM

1 (PDF) INST FOR DEFNS ANLYS
Y MACHERET

3 (PDF) MRMC DOD BLAST INJURY RSRCH PROGRAM COOR OFC
R GUPTA
T PIEHLER
R SHOGE

2 (PDF) MRMC JTAPIC PRGM OFC
W LEI
J USCILOWICZ

4 (PDF) US ARMY AEROMEDICAL RSRCH LAB
F BROZOSKI
V CHANCEY
B MCENTYRE
D WISE

1 (PDF) DEVCOM GVSC
R SCHERER

1 (PDF) DEVCOM C5ISR
AMSRD PE
D RUSIN

2 (PDF) DEVCOM CBC
M HORSMON
N VINCELLI

1 (PDF) OSD DOT&E
J IVANCIK

5 (PDF) US NAVAL RSRCH LAB
A BAGCHI
A ILIOPOULOS
J MICHOPOULOS
K TEFERRA
X TAN

4 (PDF) DAC
FCDD DAG S
K LOFTIS
FCDD DAS LBW
G DIETRICH
FCDD DAS LBE
J GURGANUS
S SNEAD

106 (PDF) DEVCOM ARL
FCDD RLD
J RIDDICK
FCDD RLD E
A EIDSMORE
FCDD RLD FR
M TSCHOPP
FCDD RLH BA
A DAGRO
T THOMAS
FCDD RLR
D STEPP
FCDD RLR EN
R ANTHENIEN
FCDD RLW
S KARNA
J NEWILL
A RAWLETT
S SCHOENFELD
J ZABINSKI
N ZANDER
FCDD RLW B
R BECKER
J CAMPBELL
P GILLICH
C HOPPEL
B SCHUSTER
A TONGE
L VARGAS-GONZALEZ
FCDD RLW M
R BRENNEN
E CHIN
FCDD RLW MA
K BERNETICH
T BOGETTI
S BOYD
J CAIN
M NEBLETT
T PLAISTED
F RACINE
E SANDOZ-ROSADO
J SANDS
J STANISZEWSKI
E WETZEL
M YEAGER
C F YEN
FCDD RLW MB
G GAZONAS
B LOVE
P MOY
D O'BRIEN
J SIETINS
J SUN
T WALTER
FCDD RLW MC
R JENSEN
FCDD RLW MD
A BUJANDA
B CHEESEMAN
K CHO
J LA SCALA
S WALSH
FCDD RLW ME
J LASALVIA
P PATEL
S SILTON
J SWAB
FCDD RLW MF
K DARLING
S GRENDAHL
C HAINES
H MURDOCH
FCDD RLW MG
J ANDZELM
J LENHART
R MROZEK
FCDD RLW T
R FRANCART
FCDD RLW TA
S BILYK
FCDD RLW TB
S ALEXANDER
T BAUMER
A BROWN
B FAGAN
A GOERTZ
A GUNNARSSON
C HAMPTON
M KLEINBERGER
E MATHEIS
J MCDONALD
P MCKEE
K RAFAELS
S SATAPATHY
M TEGTMEYER
T WEERASOORIYA
S WOZNIAK
T ZHANG
FCDD RLW TC
J CAZAMIAS
D CASEM
J CLAYTON
C MEREDITH
L SHANNAHAN
J LLOYD
FCDD RLW TD
R DONEY
R GUPTA
B KRZEWINSKI
K MASSER
F MURPHY
C RANDOW

B SCOTT
M ZELLNER
FCDD RLW TE
M LOVE
P SWOBODA
FCDD RLW TF
T EHLERS
L MAGNESS
C MEYER
D SCHEFFLER
FCDD RLW TG
N GNIAZDOWSKI
S KUKUCK
FCDD RLW S
A WEST
FCDD RLW V
F HUGHES
FCDD RLW VA
R EMERSON
FCDD RLW VB
A HALL
FCDD RLW W
T V SHEPPARD
FCDD RLW WE
T G BROWN

4 (PDF) WHITING SCHOOL OF ENG
JOHNS HOPKINS UNIV
S BAILOOR
T D NGUYEN
B NOTGHI
KT RAMESH

5 (PDF) GEORGIA INST OF TECH
S KALIDINDI
S MARGULIES
D MCDOWELL
N THADHANI
M ZHOU

1 (PDF) DEPT OF ENGRNG SCI AND MECHANICS
VIRGINIA POLYTECHNIC INST AND STATE UNIV
R BATRA

4 (PDF) MASSACHUSETTS INST OF TECHLGY
INST FOR SOLDIER NANOTECHNOLOGIES
M J BUEHLER
R RADOVITZKY
C SCHUH
S SOCRATE

1 (PDF) DEPT OF MECHL AND NUCLEAR ENGRNG
THE PENNSYLVANIA STATE UNIV
R KRAFT

1 (PDF) INDIAN INST OF TECH
R BHARDWAJ

2 (PDF) CENTER FOR APPLIED BIOMECHANICS
UNIV OF VIRGINIA
M B PANZER
R SALZAR

1 (PDF) UCSD MAT SCI AND ENG
M MEYERS

1 (PDF) DUKE UNIV
BIOMED ENG
C R BASS

1 (PDF) UNIV OF CAPE TOWN
BLAST IMPACT & SURVIVABILITY UNIT
T J CLOETE

1 (PDF) UNIV OF OXFORD
BLAST IMPACT & SURVIVABILITY UNIT
C SIVIOUR

2 (PDF) UNIV OF CAMBRIDGE
ENG DEPT
V DESHPANDE
B LIU

4 (PDF) UNIV OF SOUTH CAROLINA
COL OF ENG
S RAJAN
S SOCKALINGAM
M SUTTON
F THOMAS

3 (PDF) DSM DYNEEMA PROTECTIVE MATERIALS
U HEISSERER
R ROZANSKY
H VAN DER WERFF

1 (PDF) IMPERIAL COL LONDON
DEPT OF PHYSICS
W PROUD

1 (PDF) DIV OF ENG AND APPL SCI
CALTECH
R RAVICHANDRAN

1 (PDF) DEPT OF AERO ENG AND ENG MECH
U TEXAS AUSTIN
K RAVI-CHANDAR

1 (PDF) AERO AND ASTRO ENG
PURDUE UNIV
W CHEN

1 (PDF) DEPT OF NEUROSURGERY
MED COL OF WISCONSIN
N YOGANANDAN

1 (PDF) SANDIA NATL LABS
B SANBORN

1 (PDF) WOLFSON SCHOOL OF MECHANICAL, ELECTRICAL, AND MANUFACTURING ENG
LOUGHBOROUGH UNIV
V SILBERSCHMIDT

1 (PDF) DEPT OF MECH AND AERO ENG
CASE WESTERN RESERVE UNIV
V PRAKASH

1 (PDF) MATERIALS SCI AND ENG
UNIV OF DELAWARE
J GILLESPI

1 (PDF) SIBLEY SCHOOL OF MECH AND AERO ENG
CORNELL UNIV
S L PHOENIX

1 (PDF) DUPONT
B VANARSDALEN

1 (PDF) DEPT OF MECH SCI AND ENG
UNIV OF ILLINOIS URBANA-CHAMPAIGN
I CHASIOTIS

1 (PDF) DEPT OF MECH ENG
UNIV OF CA SANTA BARBARA
S DALY

1 (PDF) CENTER FOR BIOENG AND BIOTECH
UNIV OF WATERLOO
D CRONIN

1 (PDF) DEPT OF MECH ENG
UNIV OF ALBERTA
J HOGAN

1 (PDF) LANGLEY RESEARCH CNTR
NASA
J CLINE

2 (PDF) LOS ALAMOS NATL LAB
E BROWN
G GRAY